NUMERICAL SIMULATION OF JEFFREY FLUID-FLOW USING ANN-LMM WITH CATTANEO-CHRISTOV HEAT FLUX IN ROTATING AND SQUEEZING DOMAINS

by

Ibrahim MAHARIQ [a,b,c,d], ***Saeed ISLAM*** [e*], ***Ishtiaq ALI*** [f], ***Kashif ULLAH*** [g], ***Mehreen FIZA*** [g], ***Hakeem ULLAH*** [g*], ***and Ali AKGUL*** [h,i,j,k*]

[a] Najjad Zeenni Faculty of Engineering, Al-Quds University, Jerusalem, Palestine
[b] University College, Korea University, Seoul, South Korea
[c] Department of Medical Research, China Medical University Hospital, China Medical University, Taichung, Taiwan
[d] Applied Science Research Center, Applied Science Private University, Amman, Jordan
[e] Department of Mechanical Engineering, Prince Mohammad Bin Fahd University, Al Khobar, Saudi Arabia
[f] Department of Mathematics and Statitics, College of Science, King Faisal University, Al-Ahsa, Saudi Arabia
[g] Department of Mathematics, Abdul Wali Khan University, Mardan, Khyber Pakhtunkhwa, Pakistan
[h] Department of Electronics and Communication Engineering, Saveetha School of Engineering, SIMATS, Chennai, Tamilnadu, India
[i] Siirt University, Art and Science Faculty, Department of Mathematics, Siirt, Turkey
[j] Applied Science Research Center, Applied Science Private University, Amman, Jordan
[k] Department of Computer Engineering, Biruni University, Topkapı, Istanbul, Turkey

Original scientific paper
https://doi.org/10.2298/TSCI2505697M

The current communication studies the artificial neural networks with Levenberg-Marquardt method (ANN-LMM) based back propagation find the solutions of thermal radiation on squeezing Jeffrey fluid-flow with heat flux in a rotating frame. Also the heat and mass transfer aspects are examined in the occurrence of the Cattaneo-Christov heat flux model (CCHFM). The governing equations of Navier-Stokes equations with the help of similarity transformation a set of boundary value problem is achived. The numerical method is along with ANN-LMM. The Jeffrey fluid is tested for accuracy in the range of E-7 to E-4 by achieving a excellent agreement with the obtainable solutions and is further authorized by error histograms and regression steps. The impact of the physical parameters on the velocity and temperature profiles are discussed briefly. The velocity profile increases with the squeezing parameter and the Deborah number, β. The velocity profile decreases for the parameters rotation, ω, and relaxation time parameters, λ_1. Temperature profile decreases for the large value of the squeezing, themal relaxation parameter, and Prandtl number. For the larger value of the Deborah number and rotation parameter, the skin friction coefficient enhance, While for the λ_1 and squeezing parameter decreases.

Key words: *ANN-LMM, squeezing flow, Jeffrey fluid, CCHFM, intelligent computing, numerical computing;*

* Corresponding authors, e-mail: sislam@pmu.edu.sa; hakeemullah1@gmail.com; aliakgul00727@gmail.com

Introduction

The most popular model for the classification of heat transfer instruments in various applicable circumstances has been the classical Fourier's heat conduction law. Heat transportation is used in a variety of industries, including atomic reactors, electronic device refrigeration, and energy fabrication. Analysis of the flow has application areas in engineering and industries in the presence of magnetic fields *i.e*, blood flow measurements, MHD generators, accelerators, to propose cooling systems with liquid metal, nuclear reactors and pumps are little examples. The law of heat conduction is initiated mainly by Fourier [1]. This relationship was updated by Cattaneo [2] by taking time for thermal relaxation. The absurdity of heat conduction is incapacitated by this phase. In addition, Christov [3] considered Oldroyd's upper convective time derivative, also known as the CCM, as a modification of the Cattaneo model. Many studies [4-6] have been performed on the CCM in recent years. Engineering, physics, biology, and material sciences all benefit from the study of squeezing flows. The study of rheometric properties of fluids has gotten a lot of attention in recent years because of its significance. There are various industrial applications. Modelling of, for example, lubrication mechanisms used in fluid squeezing [7-9], squeezing flow may also be used to model the lubrication system. Stefan [10] was the one who began the flow squeezing design. Langlois [11] looked at isothermal squeezed films and presented his results. The squeezed flow of a 2nd-grade fluid was examined by Rajagopal and Gupta [12]. Hayat *et al*. [13] used thermal energy to examine the unsteady squeezing flow of Jeffery fluid. The MHD squeezed nanofuid fow in revolving channel was discussed by Shahmohamadi [14]. Ghulam *et al*. [15] studied the entropy generation and consequences of MHD Darcy-Forchmier nanofluid-flow bounded by non-linear stretching surface. Lund *et al*. [16] studied the convective effect on MHD stagnation point flowof Casson fluid over a vertical exponentially stretching/shrinking surface and the stability analysis of micropolar fluid [17]. The stabaility and solutions analysis are extended to hybrid nanofluid with heat transfer, MHD and porous effects in [18-20]. Although the aforementioned literature on the flow model is comprehensively studied by incorporating the strengths of different numerical and analytical deterministic methods. But there is need to search and utilize the stochastic numerical technique based on intelligent computing paradigms to solve and analyze the aforementioned problems. Khan *et al*. [21, 22] and Ullah *et al*. [23-25] developed the stochastic method for the COVID-19 and for various flow problems. These intelligent computing techniques for the analysis of previous different problems established the worth of intelligent computing algorithms based solvers are source of inspiration for the writers to develop a reliable soft computing structure for physical problems. The inventive highlights for the proposed intelligent computing architecture are given as:

- A new artificial intelligence based application is presented using LMM back propagation neural networks to interpret the USJFF.
- The MSE base advantage function is intended for use in the execution of ANN-LMM for approximate modelling NODE using a reference dataset that has been prepared, tested, and validated.
- The validation, testing and training procedures of NODE are developed by modelling of USJFF and association with suggestion outcome to validate the precision of the planned ANN-LMM.
- The solution of NODE via planned solver LMM is further validated through histogram plots, regression measures and convergence plots of MSE based fitness functions.

According to our literature research, to examine the flow model. The heat transfer analysis is studied via CCHFM. Proper transformation is used to obtain a NODE. We apply AI

methods through the LMM to implement non-linear back-propagation of neural networks to NODE.

Problem formulation

Assume the USJFF between two parallel plates. The lower plate is placed at $y = 0$ and stretchd with velocity $u(t) = b\gamma/1 - \delta t$. The upper plate is squeezed at $y = h(t) = y(d) = [\nu(1 - \delta t)/\gamma]^{1/2}$ in the direction lower plate. The fluid is rotating about y-axis with angular velocity $\omega = w_0/(1 - \delta t)$ with the heat flux phenomena as shown in fig. 1. The deminesnion of δ is t^{-1} and $\delta t \prec 1$. Also $T_0 > T_d$, where T_0 and T_d are the lower and upper plates temperatures. The fundamental governing equations are:

$$u_x + v_y = 0 \tag{1}$$

$$\rho\left(\frac{\partial u}{\partial t} + uu_x + vu_y + 2\omega w\right) = -p_x^* + \frac{\mu}{1+\lambda_1}\left(u_{xx} + u_{yy}\right) + \frac{\mu\lambda_2}{1+\lambda_1}\cdot$$
$$\cdot\left[u_{txx} + u_{tyy} + 2u_x u_{xx} + 2v_x u_{yx} + +u\left(u_{xxx} + u_{xyy}\right) + v\left(u_{yxx} + u_{yyy}\right) + u_y\left(u_{yx} + v_{yy}\right) + v_y\left(u_{yy} + v_{yx}\right)\right] \tag{2}$$

$$\rho\left(\frac{\partial v}{\partial t} + uv_x + vv_y\right) = -p^*{}_y + \frac{\mu}{1+\lambda_1}\left(v_{xx} + v_{yy}\right) + \frac{\mu\lambda_2}{1+\lambda_1}\cdot$$
$$\cdot\left[v_{txx} + v_{tyy} + 2v_y v_{yy} + 2u_y v_{yx} + +u\left(v_{xxx} + v_{yyx}\right) + v\left(v_{yxx} + v_{yyy}\right) + +u_x\left(u_{yx} + v_{xx}\right) + v_x\left(u_{yy} + v_{yx}\right)\right] \tag{3}$$

$$\rho\left(\frac{\partial w}{\partial t} + uw_x + vw_y - 2\omega u\right) = \frac{\mu}{1+\lambda_1}\left(w_{xx} + w_{yy}\right) + \frac{\mu\lambda_2}{1+\lambda_1}\cdot$$
$$\cdot\left[v_y w_{yy} + v_y w_{yx} + w_{xxt} + w_{yyt} + v\left(w_{yyy} + w_{yxx}\right) + \left(u_y w_{yx} + u_x w_{xx}\right) + +u\left(w_{yyx} + w_{xxx}\right)\right] \tag{4}$$

The energy equations in the form:

$$\rho c_p (V\overline{\nabla} T) = -\overline{\nabla} q \tag{5}$$

where

$$q + \lambda_3 \times\left[q_t + \left(\overline{\nabla} \times V\right) \times q - q\overline{\nabla} V\right] = -k\,\overline{\nabla} T \tag{6}$$

where λ_1/λ_2 is the arerelaxation/retardation times, ρ and c_p are the density and specific heat and is the modefied pressure, and α^* is the fractional order. Remove q from eqs.(5) and (6), energy conservation low consequent to CCHFM gives:

$$T_t + uT_x + vT_y + \tau_0 \cdot$$
$$\cdot\left[T_{tt} + uu_x T_x + vv_y T_y vuu_y T_x + 2uvT_{yx} + u^2 T_{xx} + v^2 T_{yy} + u_t T_x + 2uT_{yx} + v_t T_y + 2vT_{ty}\right] -$$
$$-\frac{1}{\left(\rho C_p\right)}\frac{\partial q_r}{\partial y} = \alpha\left(T_{xx} + T_{yy}\right) \tag{7}$$

Using the boundary conditions:

$$u_0(x) = \frac{bx}{1-\delta t},\ v = 0 = w,\ T = T_0,\ y = 0$$
$$u(d) = 0,\ v(d) = -\frac{\delta}{2}\times\left[\frac{\nu}{b\times(1-\delta\,\mathrm{t})}\right]^{1/2},\ y = d(\mathrm{t}) = \left(\frac{\nu(1-\delta\,\mathrm{t})}{b}\right)^{1/2},\ T = T_d \tag{8}$$

Remove the pressure gradient as of eqs. (4) and (5), then apply the transformation:

$$u = U_0 F'(\zeta),\ \zeta = \frac{y}{d(\mathrm{t})},\ v = -\sqrt{\frac{b\upsilon}{1-\delta t}}\,F(\zeta),\ w = U_0 G(\zeta)$$
$$\theta(\zeta) = \frac{T - T_0}{T_0 - T_d},\ \frac{\partial q_r}{\partial y} = -\frac{16T_C^3\varphi}{3\mathrm{K}}\frac{\partial^2 T}{\partial y^2} \tag{9}$$

We obtain the equations:

$$F''' + (1+\lambda_1)\left(F\,F''' - F'F'' - 2\omega G'\right) - \frac{sq}{2}\times(1+\lambda_1)\left(\zeta F''' + 3F''\right) +$$
$$+\beta\times\left[2F''F''' - F'F'''' + \frac{sq}{2}\times\left(5F'''' + \zeta F''''\right) - FF''''\right] = 0 \tag{10}$$

$$G + (1+\lambda_1)\left(2\omega F' - GF' - sqG - \frac{\eta sq}{2}F' + FG'\right) + \beta G'F'' - \beta FG'' = 0 \tag{11}$$

$$(1+Nr)\theta'' + \mathrm{Pr}\times\left(F\theta' - \frac{1}{2}\zeta\times sq\times\theta'\right) + \mathrm{Pr}\,\gamma\left(\begin{array}{l}\frac{1}{2}\zeta sqF'\theta' - \frac{3}{4}\zeta sq^2\theta' - \frac{1}{4}\zeta^2 sq\theta'' + \\ +\zeta\times sq\times F\theta' + \frac{3}{4}sqF\theta' - FF'\theta' - F^2\theta''\end{array}\right) = 0 \tag{12}$$

where

$$sq = \frac{\sigma}{b},\ \gamma = \frac{\tau_0 b}{1-\delta t},\ \text{and}\ \ \omega = \frac{\omega_0}{b}$$

is the squeezing, thermal relaxtion and rotation parameter, respectively and

$$\beta = \frac{\lambda_2 b}{1-\delta t}\ \text{and}\ \ \mathrm{Pr} = \frac{\nu}{\alpha}$$

are the Deborah and Prandtl number. The coefficient of skin friction:

$$C_F = \frac{(T_{xy})_{y=0}}{\rho U_w^2} \tag{13}$$

and

$$\mathrm{Re}_x = \frac{U_w x}{\nu}$$

is the Reynold number and

$$Nr = \frac{4T_c^3\varphi}{k\mathrm{K}}$$

is the thermal radiation parameter.

Numerical experimentation with discussion

The outcome of ANN-LMM for Case 3 of Cases 1-7 scenarios in expressions of performance and state are exposed in figs. 1(a) and 1(b), fitting and error histograms of the solution for particular Cases 1-6 are illustrated in figs. 1(c) and 1(d). The analysis of the regression is shown in fig. 1(e), for relevant six cases of flow model. furthermore, the convergence achieve parameter in expressions of MSE, implement epoch, performance, back propagations evaluate and time of completing are tabulate in tab. 1, for all three cases of every scenarios of flow mod-

el. In the subfigures 1(a), convergence of MSE for traing, validation and testing procedure are presented for Case 3 of Cases 1-7 scenarios flow model. As has been shown, the best network performance was attained at $5.4219 \cdot 10^{-09}$ at epoch 292. The, respectively values of gradient and step size Mu of back propagation are approximately $9.968 \cdot 10^{-08}$ and 10^{-09} as shown in subfigures 1(b).The performance of ANN-LMM generate results are check with mention numerical results for Case 3 of all scenarios and respective outcome are known in subfigures fig. 1(d) beside with input error dynamics of between 0,1 with step size of 1/100. The maximum error realize by the planned ANN-LMM for testing, traing, and validation data is less than $1 \cdot 10^{-04}$ for Case 3 of 1-6 scenarios of framework model. Error histograms for every input point are used to further test the error dynamics, and the outcomes are shown in subfigure 1(c), for Case 3 of Scenario 1-6, respectively, of flow model. There are errors in the error bin with the reference zero line around $4.57 \cdot 10^{-05}$ for all six scenarios of flow model. Co-relation experiments are used in regression studies to analyze the data.The outcome of regression production given in fig. 1(e) for Scenarios 1-6 of flow model. Correlations R value are always around unity *i.e*, required values for wonderful modelling, for the testing, training and validation, which recognized the exact working of ANN-LMM for solving flow model. The results of numerical experimentation for ANN-LMM for flow model equation. The ANN-LMM architecture is implemented for six scenarios. Only one scenario can be changed in each case; all other scenarios are fixed, as shown in tab. 2. The performance of ANN-LMM is around 10^{-09} to 10^{-11}, 10^{-12} to 10^{-11}, 10^{-14} to 10^{-11}, 10^{-12} to 10^{-11}, 10^{-12} to 10^{-11}, and 10^{-12} for respective Scenarios 1-6 cases of flow model. These outcome represent the dependable performance of ANN-LMM for solving flow model.

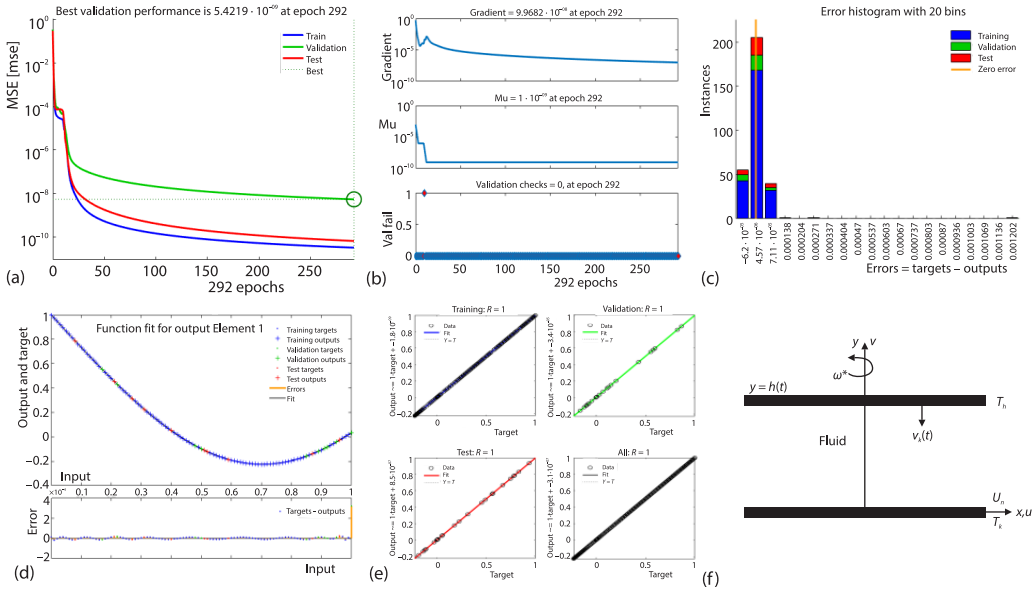

Figure 1. Outcomes of ANN-LMM; (a) performance outcome of MSE, (b) state transition dynamic, (c) error histogram, (d) fit study, (e) regression figure, and (f) schematic diagram of the flow

Velocity and temperature profiles

This subsection aims to examine how various embedding parameters influence the velocity components $F'(\zeta)$, $G(\zeta)$, and the temperature distribution $\theta(\zeta)$. As shown in the fig. 2(a), increasing the Deborah number, β, results in increasing fluid velocity $F'(\zeta)$ adjacent to

Table 1. Results of ANN-LMM for Scenario 1 of foir U2D-SJFF

Case	MSE			Performance	Gradient	Mu	Epoch	Time
	Training	Validation	Testing					
1	$1.05305\cdot10^{-09}$	$5.46518\cdot10^{-08}$	$1.22534\cdot10^{-09}$	$1.05\cdot10^{-09}$	$9.90\cdot10^{-08}$	$1.00\cdot10^{-08}$	186	0:00:02
2	$5.74882\cdot10^{-11}$	$4.15160\cdot10^{-10}$	$2.51850\cdot10^{-09}$	$5.74\cdot10^{-11}$	$9.97\cdot10^{-08}$	$1.00\cdot10^{-09}$	172	0:00:0
3	$3.27483\cdot10^{-11}$	$5.42189\cdot10^{-09}$	$6.63421\cdot10^{-11}$	$3.27\cdot10^{-11}$	$9.97\cdot10^{-08}$	$1.00\cdot10^{-09}$	192	0:00:40

Table 2. For flow model there is an explanation of the scenario as well as illustrations

Scenario	Case			Physical quantities				
		β	sq	λ_1	ω	Nr	γ	Pr
	1	0.0	1.0	2.0	0.2	1.0	1.5	2
1	2	0.5	1.0	2.0	0.2	1.0	1.5	2
	3	1.2	1.0	2.0	0.2	1.0	1.5	2
	1	1.0	0.1	2.0	1	1.5	2	1
2	2	1.0	0.2	2.0	1	1.5	2	1
	3	1.0	0.3	2.0	1	1.5	2	1
	1	1.5	1.0	1	1.5	1.5	2	2
3	2	1.5	1.0	2	1.5	1.5	2	2
	3	1.5	1.0	3	1.5	1.5	2	2
	1	1.0	2.0	1.3	0.1	1.5	2.2	1.2
4	2	1.0	2.0	1.3	0.2	1.5	2.2	1.2
	3	1.0	2.0	1.3	0.3	1.5	2.2	1.2
	1	1.2	1.2	2	1	1	2	2
5	2	1.2	1.2	2	1	2	2	2
	3	1.2	1.2	2	1	3	2	2
	1	1.3	1	2.2	2	1.5	1	1
6	2	1.3	1	2.2	2	1.5	2	1
	3	1.3	1	2.2	2	1.5	3	1
	1	0.5	1.0	1.5	0.2	1.5	–6	1
7	2	0.5	1.0	1.5	0.5	1.5	2	2
	3	0.5	1.0	1.5	0.5	1.5	2	3

the stretching plate, whereas the velocity $F'(\zeta)$ decreasing near the squeezing plate. This is credited to the raised elastic nature of the fluid at larger β values, which overall causes the velocity profile to rise. Figure 2(c) show the effect of the β in $G(\zeta)$. The volues of Deborah number increases the velocity profiles also incrases. Figures 2(e) and 2(g) shows the influence of squeezing parameter, sq, on the velocity profile $F'(\zeta)$ and $G(\zeta)$. Boths the velocity profiles increasing for the increasing the volues of sq. The effect of sq on the temperature profile, $\theta(\zeta)$, is shown in fig. 2(i). The temperature field, $\theta(\zeta)$, increases for the higher volues of the sq. Physically, increasing the sq intensifies the squeezing force exerted on the fluid, which in turn leads to a rise in the temperature distribution. Figure 2(k) show the impact of the parameter, λ_1, which is the ratio of relaxation retardation time, on the velocity profile. Fascinatingly, its influence is the reverse of what is observed for β and ω. In the fig. 2(m) show the effect of the λ_1 on the $G(\zeta)$, Velocity profile $G(\zeta)$ increases for the increasing the volues of λ_1. The effect of the rotation constraint, ω, on the velocity field is depicted in figs. 2(o) and

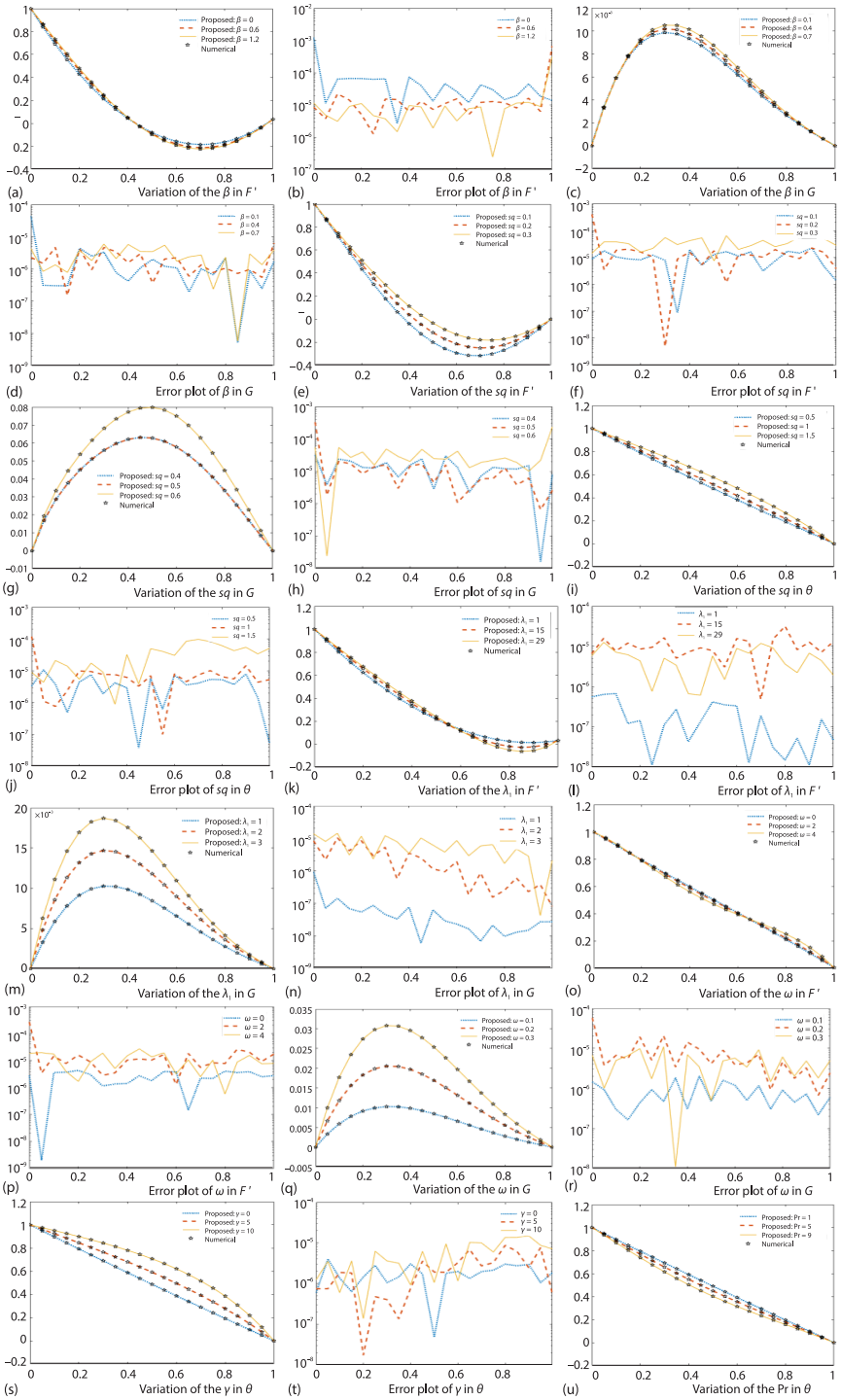

Figure 2. Show the results of different parameter on the velocity and temperature field

2(q). It is observed that with higher values of ω, the velocity field increases near the stretching plate but decreases near the squeezing plate. This is because an upsurge in ω introduces superior resistance to fluid motion, there by dropping the velocity distribution. Moreover, the velocity component $G(\zeta)$ exhibits a increasing trend with growing ω. Figure 2(s) illustrates the effect of the thermal relaxation constraint, γ, on the $\theta(\zeta)$. Clearly the temperature field increasing function of the thermal relaxation parameter. Figure 2(u) describes the result of the Prandtl number on the temperature profile, revealing a decreasing trend in temperature as Prandtl number increases. As shown in tab. 3, when *sq* and λ_1 increase, the skin friction coefficient goes down, while it rises for higher values of ω and β. Consequently, the outcome of ANN-LMM are finding for the $F(\zeta)$, $G(\zeta)$, and $\theta(\zeta)$ for all scenarios. Result of these profiles are shown in fig. 2 for Scenario 1-6, respectively of U2D-SJFF. The outcome of ANN-LMM co-ordinated with standard OHAM solutions in every case of all scenarios, consequently, in command to entrée the accuracy estimate, absolute error as of reference solution are find and results are exposed in subfigs. 2(b), 2(d), 2(f), 2(h), 2(j), 2(l), 2(n), 2(p), 2(r), 2(t), and 2 (b) for case study 1-6, respectively. We notice that absolute error are around 10^{-03} to 10^{-06}, 10^{-05} to 10^{-07}, 10^{-04} to 10^{-05}, 10^{-03} to 10^{-08}, 10^{-04} to 10^{-06}, 10^{-05} to 10^{-06}, 10^{-05} to 10^{-06}, 10^{-04} to 10^{-05}, 10^{-08} to 10^{-05}, 10^{-05} to 10^{-07}, and $10^{-0}6$ to 10^{-08}, respectively for all scenarios. All these numerical and graphical representations demonstrated the accuracy, convergent and strong performance of ANN-LMM total approach for solving the variation of flow model.

Table 3. Skin friction coefficient values of β, λ_1, ω, and *sq* in case $\gamma = 1$, Pr = 1

β	λ_1	ω	*sq*	$-C_F\sqrt{\mathrm{Re}_x}$
0.50	1	0.5	-0.10	2.633
			0	2.65
			0.10	2.63
0.50	1	0	1	1.312
		0.50		1.259
		0.90		1.216
0.50	0	0.50	1	2.38
	1			1.25
	1.5			1.03
0	1	0.5	1	0.619
0.10				0.798
0.20	1	0.5	1	0.877

Conclusiones

The following are the main points of the new initiative.

- Velacity profile increases for the squeezing parameter and Deborah number, β, and for the rotation and relaxation time parameter, ω, λ_1 the velocity profile decreases.
- Temperature profile decreases for the larg value of the squeezing, themal relaxation parameter and Prandtl number.
- For the larger value of the Deborah number and rotation parameter, the skin friction coefficient enhance, While for the λ_1 and squeezing parameter *sq*, it decreases.see tab. 3.
- The *Nr* have the same effect as Prandtl number.

References

[1] Fourier, J. B., *Théorie analytique de la chaleur*, Oeuvres de Fourier, Didot, Paris, France, 1822, 1
[2] Cattaneo, C., Sulla conduzione del calore, *Atti Sem. Mat. Fis. Univ. Modena*, *3* (1948), pp. 83-101
[3] Christov, C. I., On Frame Indifferent Formulation of the Maxwell-Cattaneo Model of Finite-Speed Heat Conduction, *Mechanics Research Communications*, *36* (2009), 4, pp. 481-486
[4] Hayat, MT., *et al*., Impact of Cattaneo-Christov Heat Flux Model in Flow of Variable Thermal Conductivity Fluid over a Variable Thicked Surface, *International Journal of Heat and Mass Transfer*, *99* (2016), Aug., pp. 702-710
[5] Acharya, *N*., *et al*., Cattaneo-Christov Intensity of Magnetised Upper-Convected Maxwell Nanofluid-Flow over An Inclined Stretching Sheet: A Generalised Fourier and Fick's Perspective, *International Journal of Mechanical Sciences*, *130* (2017), Sept., pp. 167-173
[6] Han, S., L., *et al*., Coupled Flow and Heat Transfer in Viscoelastic Fluid with Cattaneo-Christov Heat Flux Model, *Applied Mathematics Letters*, *38* (2014), Dec., pp. 87-93
[7] Gupta, P. S., Gupta, A. S., Squeezing Flow between parallel Plates, *Wear*, *45* (1977), 2, pp. 177-185
[8] Törnqvist, R., *et al.*, Non-Isothermal Process Rheology of Thermoplastic Composites for Compression Flow Moulding. Composites Part A: *Applied Science and Manufacturing*, *31* (2000), 9, pp. 917-927
[9] Shirodkar, P., *et al.*, Lubrication Flows in Viscoelastic Liquids: 2 Effect of Slip on Squeezing Flow between Approaching Parallel Rigid Planes, *Chemical Engineering Communications*, *14* (1982), 3-6, pp. 151-175
[10] Stefan, M. J., *Versuch Uber die scheinbare adhesion*, Akademie der wissenschaften in Wien, Mathematisch-Naturwwissenschaftliche, Wien Austia, 1874
[11] Langlois, W. E.,Isothermal Squeeze Films, *Quarterly of Applied Mathematics*, *20* (1962), 2, pp.131-150
[12] Rajagopal, K. R., Gupta, A. S., On a Class of Exact Solutions to the Equations of Motion of a Second Grade Fluid, *International Journal of Engineering Science*, *19* (1981), 7, pp. 1009-1014
[13] Hayat, T., *et al.*, Thermal Radiation Effects In Squeezing Flow of a Jeffery Fluid, *The European Physical Journal Plus*, *128* (2013), 8, pp. 1-7
[14] Shahmohamadi, H., Rashidi, M. M., The VIM Solution of Squeezing MHD Nanofluid-Flow in a Rotating Channel with Lower Stretching Porous Surface, *Advanced Powder Technology*, *27 (*2016), 1, pp. 171-178
[15] Ghulam, R., *et al*., Shehzadi, Entropy Generation and Consequences of MHD Darcy-Forchmier Nanofluid-Flow Bounded by Non-Linear Stretching Surface, *Symmetry*, *12* (2015), 4, 652
[16] Lund, L. A., *et al*., Convective Effect on MHD Stagnation Point Flowof Casson Fluid over a Vertical Exponentially Stretching/ Shrinking Surface, *Symmetry*, *12* (2015), 1238
[17] Lund, L. A., *et al.*, Triple Solutions and Stability Analysis of Micropolar Fluid-Flow on an Exponentially Shrinking Surface, *Crystals*, *10* (2017), 283
[18] Lund, L. A., *et al.*, Rotating 3-D Flow of Hybrid Nanofluid on Exponentially Shrinking Sheet, *Symmetry*, *12* (2016), 1637
[19] Lund, L. A., *et al*., *et al*., Magnetized flow of Cu + AI_20_3 + H_2O Hybrid Nanofluid in Porous Medium, *Stability and Duality Analysis, Symmetry*, *12* (2016), 1513
[20] Nisar, K S., *et al*., Exploaration of Alumenium and TitaniumAlloys in the Stream Wise and Secondary Flow Directions Comprising the Siginificant Impacts of MHD Hybrid Nanofluid, *Crystal*, *10* (2016), 679
[21] Khan, R. A., *et al*., Heat Transfer between Two Porous Parallel Plates of Steady Nanofludis with Brownian and Thermophoretic Effects: A New Stochastic Numerical Approach, *International Communications in Heat and Mass Transfer*, *126* (2021), 105436
[22] Khan, A., *et al*., Stationary Distribution and Extinction of Stochastic COVID-19 Epidemic Model, Fractals, *30* (2022), 1, 2240050
[23] Ullah, H., *et al*., A Levenberg-Marquardt Backpropgation Method for Boundary-Layer and Heat Transfer of Oldroyd B Nanofluid-Flow over a Stretching Sheet, *Computer Intelligence and NeuroScience*, *2022* (2022), 2546879
[24] Ullah, H., *et al.*, Falkner-Skan Equation with Heat Transfer: A New Stochastic Numerical Approach, *Mathematical Problems in Engineering*, *2021* (2021), 3921481
[25] Ullah, H., *et al*., Levenberg-Marquardt Backpropagation for Numerical Treatment of Micropolar Flow in a Porous Channel with Mass Injection, *Complexity*, *2021* (2021), 5337589

Paper submitted: February 10, 2025
Paper revised: June 17, 2025
Paper accepted: July 23, 2025